NASA/TM–2019–220197

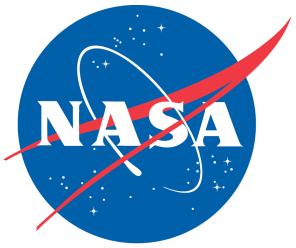

Computational Non-destructive Evaluation Improving Ultrasonic Interrogation of Complex Geometry Composite Parts

V. Hafiychuk
Stinger Ghaffarian Technologies, NASA Ames Research Center, Moffett Field, CA

K. R. Wheeler
Intelligent Systems Division, NASA Ames Research Center, Moffett Field, CA

K. Gee
Advanced Supercomputing Division, NASA Ames Research Center, Moffett Field, CA

March 2019

NASA STI Program. . . in Profile

Since its founding, NASA has been dedicated to the advancement of aeronautics and space science. The NASA scientific and technical information (STI) program plays a key part in helping NASA maintain this important role.

The NASA STI Program operates under the auspices of the Agency Chief Information Officer. It collects, organizes, provides for archiving, and disseminates NASA's STI. The NASA STI Program provides access to the NASA Aeronautics and Space Database and its public interface, the NASA Technical Report Server, thus providing one of the largest collection of aeronautical and space science STI in the world. Results are published in both non-NASA channels and by NASA in the NASA STI Report Series, which includes the following report types:

- TECHNICAL PUBLICATION. Reports of completed research or a major significant phase of research that present the results of NASA programs and include extensive data or theoretical analysis. Includes compilations of significant scientific and technical data and information deemed to be of continuing reference value. NASA counterpart of peer-reviewed formal professional papers, but having less stringent limitations on manuscript length and extent of graphic presentations.
- TECHNICAL MEMORANDUM. Scientific and technical findings that are preliminary or of specialized interest, e.g., quick release reports, working papers, and bibliographies that contain minimal annotation. Does not contain extensive analysis.
- CONTRACTOR REPORT. Scientific and technical findings by NASA-sponsored contractors and grantees.
- CONFERENCE PUBLICATION. Collected papers from scientific and technical conferences, symposia, seminars, or other meetings sponsored or co-sponsored by NASA.
- SPECIAL PUBLICATION. Scientific, technical, or historical information from NASA programs, projects, and missions, often concerned with subjects having substantial public interest.
- TECHNICAL TRANSLATION. English-language translations of foreign scientific and technical material pertinent to NASA's mission.

Specialized services also include organizing and publishing research results, distributing specialized research announcements and feeds, providing information desk and personal search support, and enabling data exchange services.

For more information about the NASA STI Program, see the following:

- Access the NASA STI program home page at `http://www.sti.nasa.gov`
- E-mail your question to `help@sti.nasa.gov`
- Phone the NASA STI Information Desk at 757-864-9658
- Write to:
  NASA STI Information Desk
  Mail Stop 148
  NASA Langley Research Center
  Hampton, VA 23681-2199

NASA/TM–2019–220197

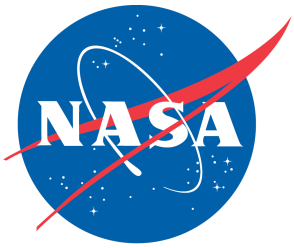

Computational Non-destructive Evaluation Improving Ultrasonic Interrogation of Complex Geometry Composite Parts

V. Hafiychuk
Stinger Ghaffarian Technologies, NASA Ames Research Center, Moffett Field, CA

K. R. Wheeler
Intelligent Systems Division, NASA Ames Research Center, Moffett Field, CA

K. Gee
Advanced Supercomputing Division, NASA Ames Research Center, Moffett Field, CA

National Aeronautics and
Space Administration

Ames Research Center
Moffett Field, California

March 2019

Acknowledgments

The authors would like to thank the NASA Advanced Composites Project for support and also for enabling the partnership between Boeing and NASA researchers. The authors are grateful to the Stefan Schuet for a valuable comments that improved the manuscript.

Available from:

NASA STI Program / Mail Stop 148
NASA Langley Research Center
Hampton, VA 23681-2199
Fax: 757-864-6500

Abstract

Finite element simulation was employed in modeling the ultrasound (UT) pressure pulse propagation through a coupled liquid-composite medium to reproduce experimental data. From the simulation point of view, the proposed approach is challenging when there is a large simulation domain. For example, it is shown that a sub-micron wavelength of an ultrasonic wave requires a mesh size of several microns and this in turn requires significant computational resources, as well as special care in modeling. Some of the simulation results are presented considering that such modeling should reproduce experimental data for a healthy and faulty composite structure with complex geometry. Many possible experimental setups are simulated to demonstrate the non-destructive testing technique. This setup includes the generation of pressure pulse propagating through the tested composite plate and possible scattering by discontinuities (area of different impedance) that may be present in the panel. This scattered pulse together with the baseline pressure pulse generates a signature on the probe element which can be used to locate the position of defects in the structures.

1 Introduction

Nowadays manufacturing technologies in aerospace industry allow the production of complex composite panels (see, for example, Fig. 1). These complex structures create substantial inspection challenges. For example, variable curvature and material thickness lead to manual inspection and require huge labor cost. At the same time, automated inspections by robotics are difficult not only because the complex geometry limits access to the structure surface, but also by correct interpretation of the discerning faults in a structure that is variable in shape and thickness.

At the same time, understanding of the physics of ultrasounic nondestructive techniques based on phased-arrays enables development of inspection automation despite part-to-part variability of the structures. In this case, the optimization of the detection technique requires additional knowledge about the physics of the wave propagation and scattering from a fault in order to single out a faulty signal from noise. In fact, manufacturing variability and surface roughness can often alter the detection features, and development of simulation tools for fault detection and diagnostics is an important part of the solution to the problem. Together, experimentation and simulation approaches might greatly improve the understanding of detection features for composite structures with complex geometries.

The demand of mass production makes automation of inspection strategies a first priority and forces us to develop a suitable simulation approach NDE of such structures. The combination of experimental work with the results of modeling makes it possible to optimize the inspection technique, increase the confidence in fault detection strategy, as well as find the most cost-effective solution of such challenging structure. As a result, the development of the appropriate defect detection technique and automation is an important problem.

This report explores the utility of computational non-destructive evaluation

(CNDE) to predict and ultimately recommend methods for ultrasonic interrogation of composite parts with complex geometries. The predictions are utilized to recommend alternative configurations for interrogation intended to result in an improved understanding of defect discovery and quantification. The objective of this work is to streamline certification and manufacturing processes development by optimizing NDE parameters to better quantify flaws in complex geometries. The hope is to minimize the number of time consuming and expensive prototype NDE qualification parts that need to be created. This increases throughput efficiency during manufacture of structural elements, subcomponent level, and full-scale test articles.

The subject of this study is a composite part selected jointly by NASA and Boeing personnel. Complex curvature and difficulty for NDE interrogation were the main selection criteria. The selected part is shown in Figure 1. It resembles a saddle with the sharpest radius of curvature varying from 12.7 to 16.5 cm, and it will be referred to as the "Saddle" part throughout this report. The part is 113cm in length composed of IM7-8552 with 32 layers. The layup was: 45/90/-45/0/45/90/-45/0/45/90/-45/0/0/-45/90/45/0/-45/90/45/0/...

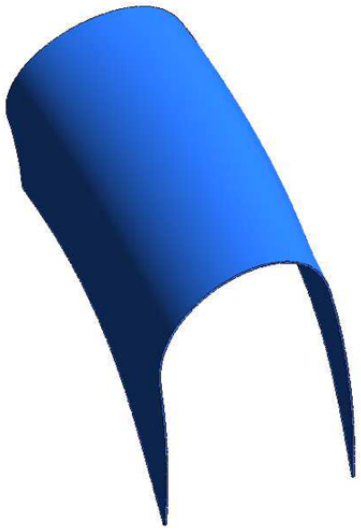

Figure 1. The Boeing saddle part which is highly curved and 113cm long

The saddle part was interrogated with a proprietary robotic system that could move an ultrasonic water bubbler head along the surface of the part. An Olympus Focus PX phased array and conventional ultrasonic data acquisition instrument was used to generate and receive signals [1] to and from the 64 element, 0.5mm pitch water bubbler head with a 2.0in water path. The saddle part was interrogated in a water tank, although due to its size, much of the part was above the water line. This meant that the back side of the part under interrogation could be above the water line and cause a greater reflection impedance than would be expected if it were under water.

In order to simulate the pressure waves that are induced in the water path

by the pulse signal, it was necessary to understand the transfer function of the transducer array that translates the voltage waveforms into pressure waveforms in the water path. With this in mind, Boeing developed an experimental setup with a water bubbler head submerged in water. A second set of transducers were attached directly to the face of the head. This transmission experiment then activated each of the head's transducers one at a time, and then the signal was received on all of the transducers on the second array. An example of the collected data is shown in Figure 2. The bandwidth employed in this experiment was 2.25MHz.

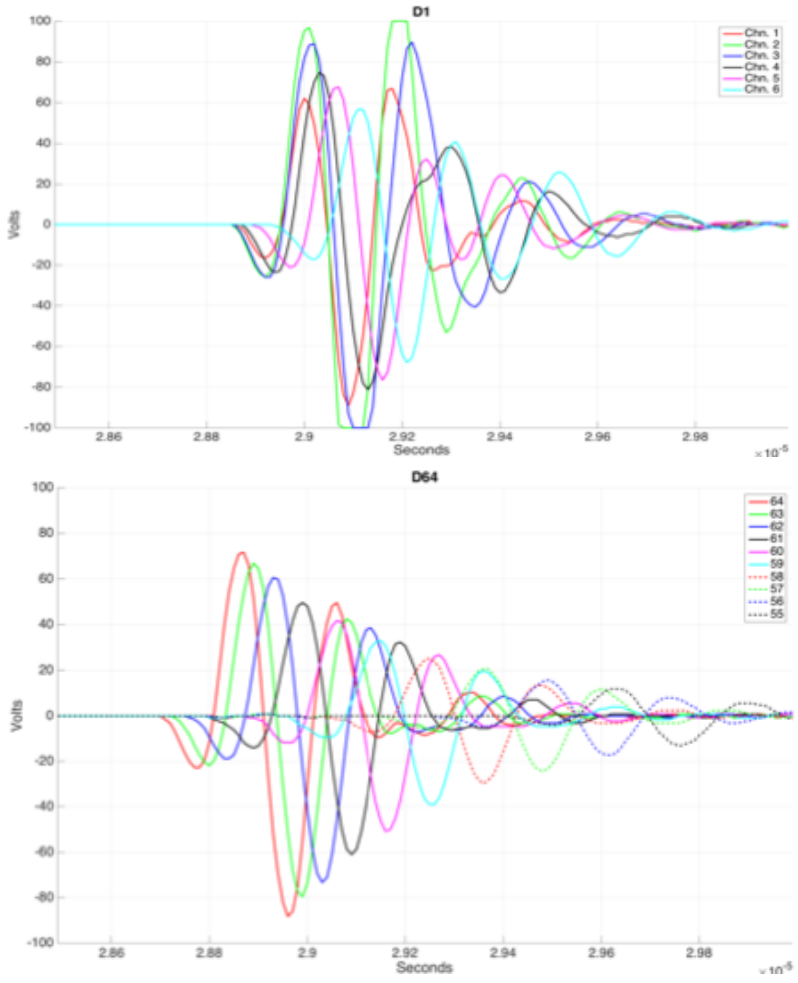

Figure 2. Calibration Signals – Top: Channel 1 is source, channels 1-6 of received signal shown, Bottom: Channel 64 is source, channels 55 – 64 of received signal shown.

A calibration experiment was conducted to understand how to formulate a pressure source signal in the computational simulation which will be discussed later. Observe that there is a variation between channels due to the characteristics of the

bubbler head geometry. Symmetries that would be expected, such that the signal transmitted from channel 1 will be mirror symmetrical to the signal received from channel 64, were not exactly true. It was not the intention to replicate such issues in the computational domain, but instead to understand that there was such variability in shape which could influence further observations.

For the first data set the bandwidth of the interrogation signal was 2.25MHz. The head was operated such that only a single element was pulsed at a time, and then the echo was received on all of the channels. The second data set used three different frequencies: 1.0MHz, 2.25MHz, and 5.0MHz. The channels were operated either individually as mention above, or in phased arrays of 4 elements.

2 First Data Set Analysis

The curvature makes inspection of the part difficult in the water tank. The robotic system that Boeing developed was capable of moving a water bubbler ultrasonic head along the convex surface of the curve. The difficulty was that the smooth tool-side of the part was the inside concave surface. Thus, the head was moved along the unusually rough convex side resulting in the head having a variable distance from the front surface. An example of this roughness appears in Figure 3 where the first reflection is not a straight line but rather has great waviness. Although the time of flight from head to surface could be corrected, the variability in the interrogation has the potential to mask reflections due to faults near the surface.

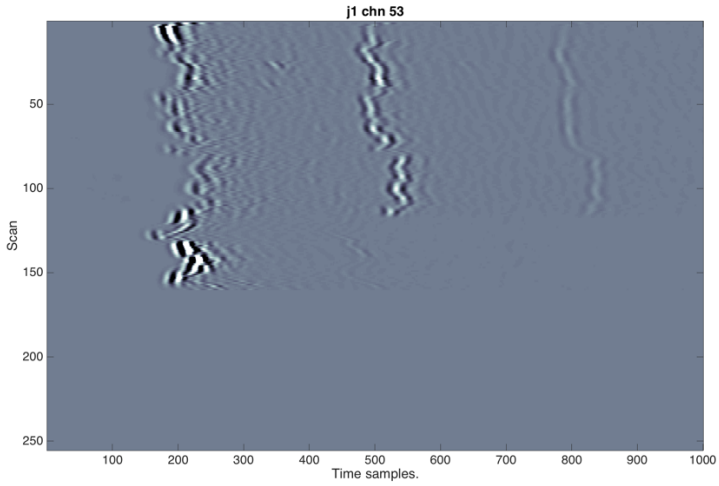

Figure 3. The first reflections (left most) from the surface are wavy instead of straight due to the rough surface causing the interrogation head to be a variable distance from the actual front surface. This level of variability makes time-of-flight and thus depth calculations complicated.

The potential for a fault near the surface (closest to the interrogation head)

to be masked is demonstrated in Figure 3 where the second reflection (from the backside) disappears. Due to the irregularity of the front side edge, it is difficult to determine if there is a fault causing this or if there was some other issue with the data collection.

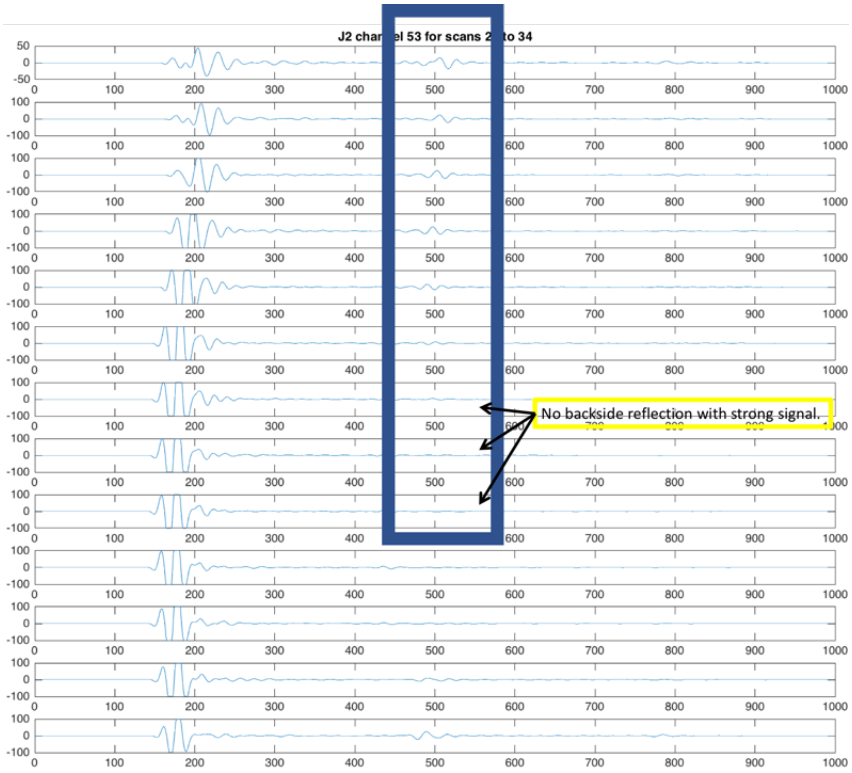

Figure 4. The disappearance of the backside reflection potentially indicates that most of the interrogation energy was absorbed/scattered near the surface due to a sub-surface fault.

The dominant feature of the first data set was a result of the severe surface roughness of the part. Because of this, our first recommendation was to develop a method to position the ultrasonic bubbler head on the concave side of the surface, which was the tool-side, and thus smooth. Through a round-table discussion between Boeing and NASA, it was determined that modeling the rough surface of the part was not of interest because the amount of roughness seen on the part was not representative of panels in manufacturing.

Another observation from the first data set was that the back-side reflection would disappear due to something (roughness, delamination) near the surface. Understanding the limits of detectability for near-surface faults was of interest. The second recommendation was to try higher frequencies for interrogation so that the wavelengths would be finer and thus be able to highlight and localize faults of a similar size to the wavelength. This recommendation resulted in collecting data at 5.0MHz for the second data set. In this sampling setup, depth of penetration

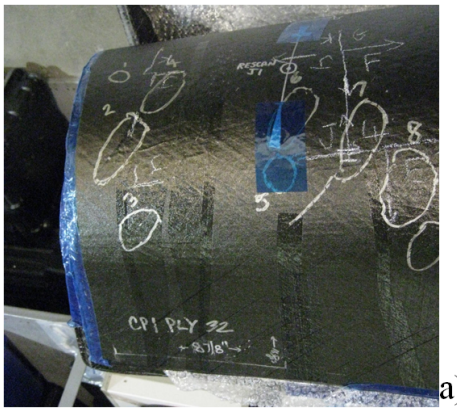

a)
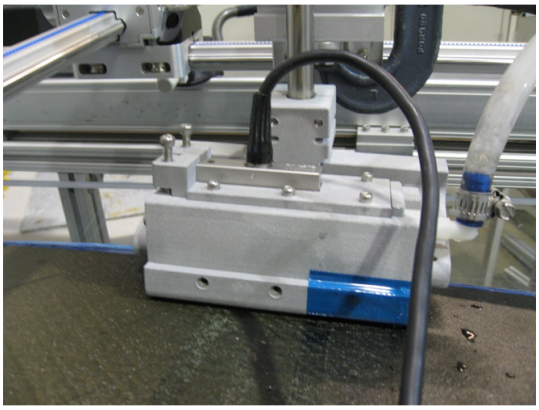
b)

Figure 5. Saddle panel view - (a) and moving water tank with ultrasonic probe – (b)

and dispersion did not seem to prevent utilization of 5.0MHz. For rough-side part inspections, a lower frequency (1.0MHz) with wavelength larger than the surface roughness was tried. This had the obvious disadvantage of reducing the fault detection resolution.

3 NDE approach: Pressure Wave Propagation and Detection Experiment

Ultrasonic non-destructive evaluation relies on the analysis of echo signals for fault detection [2–5]. The pulse echo method in particular, relies on the measurement of time-of-flight through the thickness of the material. This method is ideally fitted to detect macroscopic defects in the test composite specimens. The problem encountered here is that an air gap between the UT probe and inspected structure needs to be removed to maximize sound energy penetration. In this case, the typical solution in NDE practice is to use a couplant between the probe and the inspected material. Water makes for a good practical couplant. The part and transducer should then be connected by water only. A simple way to achieve this is by immersing the whole part in a water tank, but this is not always possible. A practical solution for large parts is to flow water through the probe head during inspection over a water tank. In this report finite element (FE) simulation is used to model and analyze this method. Our objective is to develop a deeper understanding of the method itself, and the parameters that can be used to optimize it.

The experimental equipment for testing a saddle composite panel by UT is presented in Fig. 5. The experimental measurement of UT scans of the saddle part are presented in Fig. 6, 7, 8.

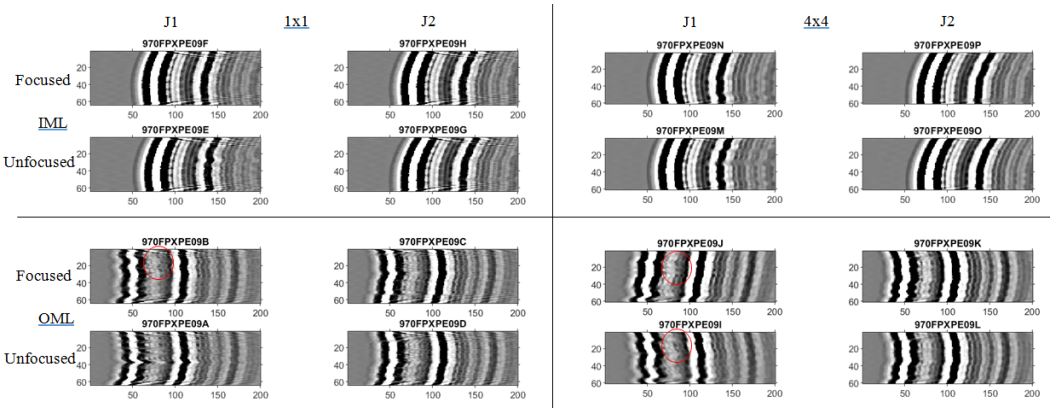

Figure 6. Olympus Focus PX B-scan of the saddle part with frequency of 1MHz

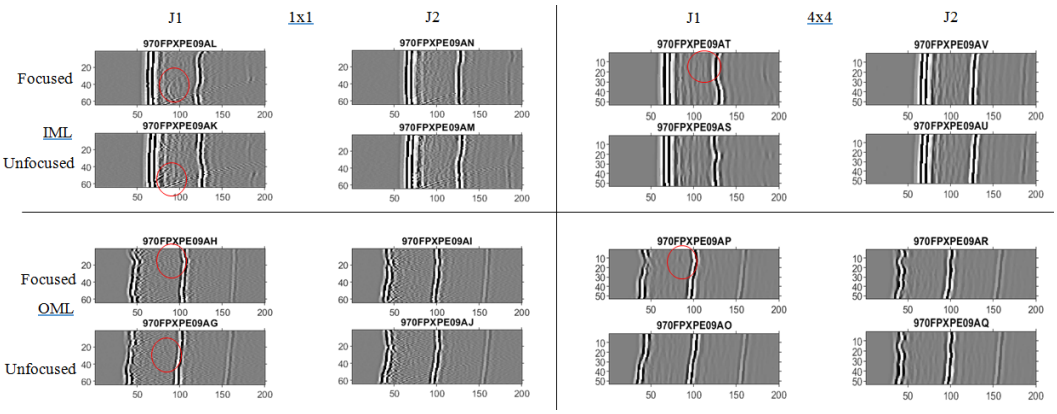

Figure 7. Olympus Focus PX B-scan of the saddle part with frequency of 3.5MHz

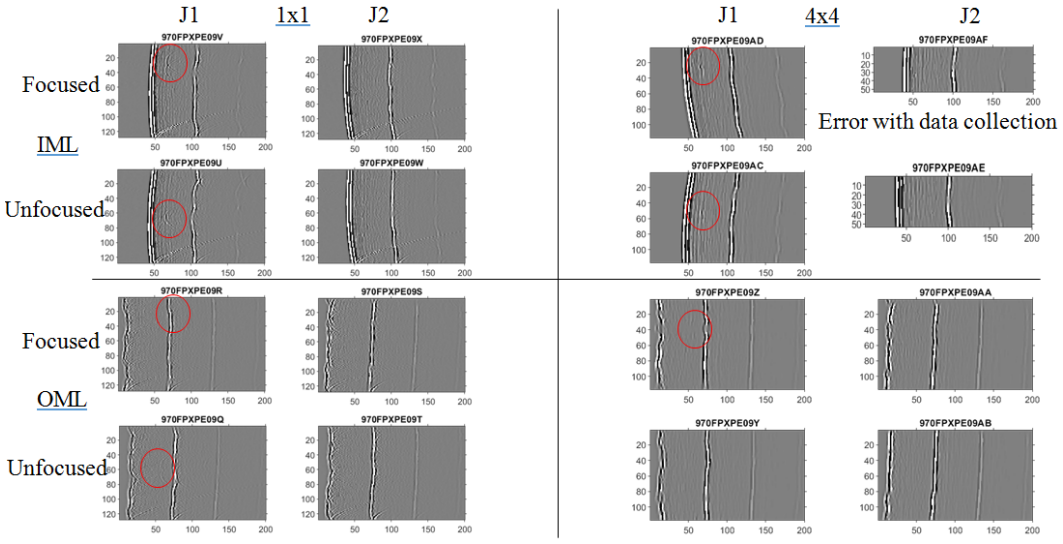

Figure 8. Olympus Focus PX B-scan of the saddle part with frequency of 5MHz. The red circles show strong signals reflected from the defect

4 Physics-based Analysis of the Experiment

Solid phantom determination. The experimental setup considered here has a 2in water path through the ultrasonic head to the composite part. The UT pressure pulse is normal to the part surface.

To verify the feasibility of the proposed simulation approach, the time-domain plots will be compared with A scans obtained from cross-sections of B-scan data (for certain values of y in B-scan). Figure 9a shows a schematic diagram of the experimental setup used.

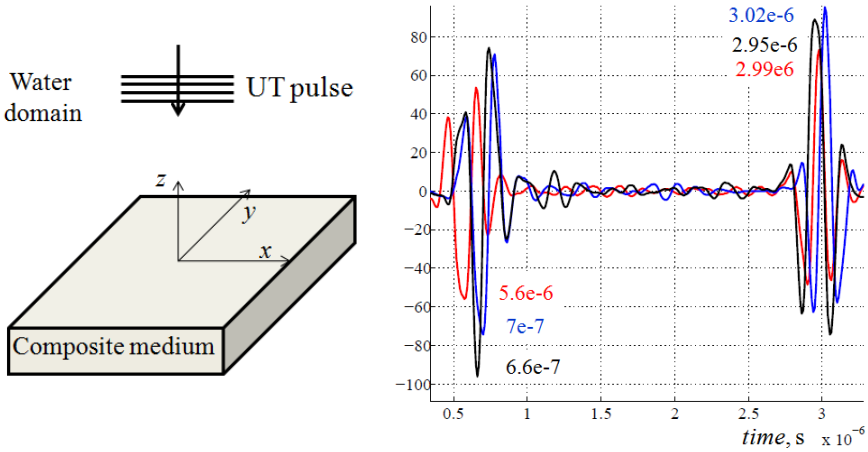

(a) (b)

Figure 9. Schematic view of the experiment – (a), and A-scan signal on the probe simulated for composite plate without delamination – (b)

The boundary conditions at the water composite interface require that the normal displacement and the normal stress are continuous through the interface. The particles normal to the surface velocity in the water are equal to the normal displacement velocity in the solid.

For the pulse echo technique the composite material is substituted by phantom medium with the same thickness that produces the same time of flight in the experiment (Fig 9 b). In the composite plate with ultrasound phantom, the speed of sound is the same as that in the composite plate. From the time of flight view the plate is considered a homogeneous material with Young modulus E , Poisson ratio ν and density ρ. The speed of sound follows from the composite thickness d. The speed inside the phantom material is then calculated by equation 1.

For the wave propagation normal to the plate (x_3 direction, fig 9) the acoustic dynamics in anisotropic media can be decomposed into a system of three equations. The pure longitudinal wave propagates along the x_3-axis, and two pure shear waves propagate as follows: one polarized parallel to the x_1-axis and the other polarized parallel to the x_2-axis. The longitudinal wave velocity can be obtained from [5].

$$\left(c_{33} - \rho v_3^2\right) A_3 = 0, \tag{1}$$

The velocity $v_3 = \sqrt{c_{33}/\rho}$ follows from the solution of equation 1, and

$$\left(c_{55} - \rho v^2\right) A_1 = 0 \tag{2}$$

$$\left(c_{44} - \rho v^2\right) A_2 = 0 \tag{3}$$

leading to the generation of two shear waves propagating in x_1 and x_2 directions with corresponding velocities $v_1 = \sqrt{c_{55}/\rho}, v_2 = \sqrt{c_{44}/\rho}$. The effective material constants for an anisotropic elastic material are as follows in units of $10^9 N/m^2$ [5],

$$c_{11} = 160.73, c_{12} = c_{13} = 6.44, c_{22} = c_{33} = 13.92, c_{55} = c_{66} = 7.07, c_{44} = 3.5$$

Here, the x-axis is parallel to the fiber axis. The density $\rho = 1540\text{kg/m}^3$. Thus, the phase velocity of the longitudinal wave propagating in the x_3 direction is about $v_3 = 3.0$ km/s. On the other hand, phase velocities of shear waves are not needed in the 3- or 2- directions (S or SH directions) for this simulation approach.

The elastic wave propagation is found by solving the acoustic dynamics in water and the structural dynamic equation in the solid. In the composite plate ultrasound phantom, the speed of sound is the same as that in composite plate. From the time-of-flight perspective, consider that the plate is a homogeneous material with Young modulus E , Poisson ratio ν and density ρ. Having the composite thickness d, the speed of sound can be calculated. The speed inside the phantom is then calculated by equation

$$v = 2d/\tau \tag{4}$$

τ is the time-of-flight, d is the thickness of the investigated panel (is about 4.34 mm). From Fig. 9 as well as from many other experimental results, it is possible to see that the time of flight for pristine plate is about $2.3 - 2.4\mu$s, which gives us the longitudinal velocity value about 3.7m/s.

The velocity for the isotropic material is found from

$$c_L^2 = \frac{(1-\nu)E}{(1-2\nu)(1+\nu)\rho}, c_s^2 = \frac{E}{(1+\nu)\rho}. \tag{5}$$

where c_l, c_s are the longitudinal and transverse wave velocities, respectively. Using the longitudinal velocity from equation (4) and Poisson ratio of 0.3 the Young modulus can be found to be 16 GB.

If the composite panel is viewed as an acoustic phantom with density of $\rho = 1,540 kg/m^3$, then the bulk modulus is:

$$K = V^2 \cdot \rho = (3.8)^2 \cdot 1.54 \cdot 10^9 = 21\text{GPa}. \tag{6}$$

The shear modulus is equal to zero for acoustic medium.

The highest ultrasound frequency in the experiments is 5MHz. This frequency is used for high resolution fault detection, including the ability to detect faults close to the surface on both sides of the material. Using a water domain sound velocity

of 1540m/s, the sound wavelength in water for 5MHz is obtained from the simple wave relationship

$$\lambda = v/f = 1,500m/s/5 \cdot 10^{-6}s = 0.3\text{mm}.$$

It is not possible to distinguish inhomogeneties smaller than the wavelength, which gives the ultimate resolution limit. In the composite panel, this value is higher since the velocity is more than two times higher. A 500μm discontinuous embedding will not be detectable in such a UT scan.

Pulsed-echo analysis. Knowing the velocity of sound in water and in composite, the time between echoes can be used to determine the location of faults and inhomogeneities in the composite part. Consider a layered acoustic media with three different impedance's: 1 – water, 2 – composite panel and 3 – air without any fault. Assuming plane waves, the incident signal can be written as $u(t,z) = u(t-z/v)$, where v is speed of sound in water. On the water-composite interface a part of the pulse is reflected from the interface and another part penetrates the composite panel according to the acoustic impedance mismatch between the two adjacent layers. The reflected signal travels back to the probe element in the form of $u(t,z) = R_{12}u(t+z/v)$. The transmitted signal is $u_1(t,z) = T_{12}u(t-z/c)$, where c is longitudinal velocity in the composite panel, and the z-axis points downward. For the composite of thickness d, the backscattered signal $u_2(t,z) = T_{12}R_{23}T_{21}u(t-2d/c+z/v)$ is reflecting from the bottom surface and propagating in the water domain to the probe element as well.

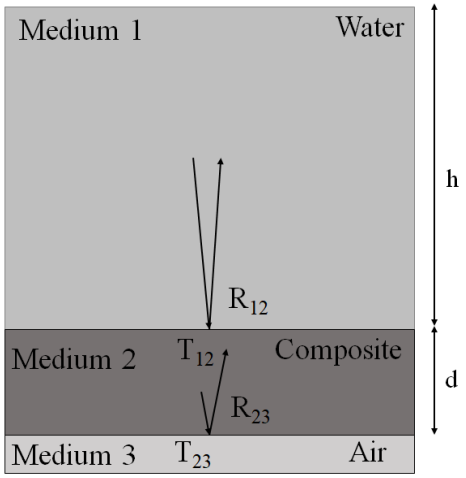

Figure 10. Schematic view of the wave propagating in water domain and composite plane.

The reflection and transmission coefficients can be found, for example, in [6]

$$R_{12} = (Z_2 - Z_1)/(Z_1 + Z_2), \quad T_{12} = 4Z_1Z_2/(Z_1 + Z_2), \tag{7}$$

where Z_1 is the acoustic impedance of the water from which ultrasound is transmitted, and Z_2 is the acoustic impedance of the composite panel (the medium in which ultrasound is transmitted). The acoustic impedance $Z = \rho c$, where ρ is the material

density and c is the speed of sound, represents the stiffness experienced by the sound wave. Rigid materials tend to have high density and ffaster speed of sound, which makes for greater impedance. If the sound is traveling from medium 1 (in our case water) with impedance Z_1 to medium 2 (composite panel) with impedance Z_2 the following relationship can be obtained: $Z_1 < Z_2$, and according to (7) part of the wave is reflected from the panel surface. In the case $Z_1 \ll Z_2$ the value of R is about 1 and the boundary is considered rigid and reflects all incident waves without a change in phase. The transmitted wave propagates through the first boundary and travelers inside the panel until the bottom boundary.

The sign of the pulse inside the panel is the same as the incident pulse in the water domain. When the pulse in the panel hits the backside of the composite panel surrounded by air the situation changes. In this case $Z_2 \gg Z_3$, and the reflection coefficient R is about minus one. While majority of the pulse is reflected from this surface and the boundary is considered soft, there is a phase shift for π. In this case the compression pulse becomes a tensile strain pulse and vice versa.

This is a simple 1D consideration. In real composite systems, subsurface delaminations and any other discontinuities depend upon their size and depth of localization and this case will be considered later.

5 Characteristic Features of the Abaqus Model

The elastic wave propagation in water and in the composite domain is performed by solving the acoustic dynamics in the water domain and the structural dynamics in the solid using ABAQUS/Explicit. One of the advantages of using Abaqus is in having acoustic and solid mesh elements conveniently positioned to simulate pressure waves and stress waves simultaneously. Moreover, a composite modulus has been incorporated that enables simulation of integrated composite parameters, especially in the curvilinear coordinate system.

The 3D and 2D models to reproduce experimental results was developed. Both approaches have limitations in usage and depend substantially on the desired features to be reproduced by computation. The simulation for the water composite system will be presented for a 2D ABAQUS/Explicit model. The time-step size of such a simulation was calculated in software by estimating the initial time-step. Typically the time step size was about 1 ps. The developed simulation of the coupled liquid/solid UT system is based on the discussion in the previous section. Two simulation approaches were used, one based on acoustic pressure, and he other based on acoustic pressure solid stress.

The Load boundary condition for pressure pulse.

In the model, a pressure force was realized by using an amplitude time-domain function, $Ampl(t)$. Mainly a 2 Hanning sine signal was employed with a carrying frequency of $f_0 = 5$MHz . The transient excitation is modeled using a cyclic single frequency pressure/force.

$$p(t) = \begin{cases} (1 - \cos(\frac{2\pi f t}{N})). & 0 < t < N/f \\ 0. & \text{otherwise} \end{cases} \tag{8}$$

where, f is the excitation wave frequency and N represents the number of cycles.

Planar nonreflecting boundary condition – The nonreflecting boundary condition available in ABAQUS is used on the side walls in the water domain. This planar boundary condition ignores the curvature of the boundary and the possibility that waves in the simulation may impinge on the boundary at an arbitrary angle. The planar nonreflecting condition provides an approximation: acoustic waves are transmitted across such a boundary with little reflection of energy back into the acoustic medium. The amount of energy reflected is small if the boundary is far away from major acoustic disturbances and is reasonably orthogonal to the direction of the dominant wave propagation [7].

Pressure load – The displacement is as follows: a Sine Hanning signal was employed in the partitioned area of the composite. The probe elements were built up at the top of the water domain center. The distributed loads on these probe elements connecting the edge of acoustic elements can be interpreted as normal pressure gradients per unit density (dimensions of force per unit mass or acceleration).

Tie constraint – The bottom edge elements of the acoustic fluid use a tie constraint to the solid element of the composite. The non-acoustic elements have properties similar to the fluid itself since these elements are replacing the fluid medium near the free surface. They should have a thickness similar to the height of the adjacent acoustic elements. This technique, realized in Abaqus, has the added advantage of providing the deformed shape of the free surface under the loading. The "structural fluid" surface and the "acoustic fluid" surface are then coupled using a surface-based mesh tie constraint. The water acoustic medium is a dominant actor and the composite is subservient.

Mesh shape elements – The mesh element AC2D3, of the quad, quad-dominated and tri for fluid mesh, and Quad plane stress CPS4R element for composite simulation were used. The typical mesh view is presented in Fig. 11, where 4-node quadrilaterals, and tri elements are displayed. A sufficiently fine mesh size is required for accurate simulation results.

From theory [7] it is recommended that more than 10 elements per wavelength are needed (mesh size of $\lambda/10 = 0.3\text{mm}/10 = 30\mu\text{m}$). For our thick water acoustic domain, reproducible results can be obtained with a mesh of about 5μm. For a larger mesh size, there is igh dispersion in the propagating signal. This means that about $10,000$ nodes are needed along the water domain thickness, and the overall model requires tremendous computational resources to evaluate.

For the 3D model, the domain needs to be at least $0.5 \times 0.5\text{mm}^2$ (size of the one element of the probe) so that the domain has another $10,000$ nodes. In this case, the symmetric boundary condition is used, since for a nonreflecting boundary condition the water pressure signal will vanish quickly. For a symmetric boundary condition in 3D, it is acceptable to have a mesh size of $\lambda/10 = 30\mu$m.

For 2D simulation, the nonreflecting boundary is a sufficiently good approximation. At the same time good results are obtained at a very fine mesh (5μm so $\lambda/60$). Such a small mesh size was impossible to realize across all of the simulation domains. To circumvent this difficulty, the central path of the pulse was meshed with fine resolution, and the side domain was meshed with coarse resolution in lat-

eral direction. Main simulation results were obtained in a case the whole width was partition for a three equidistant domain. The central part was meshed by fine mesh and two side parts with a coarse one.

The smallest homogeneous mesh size for all of the domain was 7.5μm. Acoustic elements embedded in Abaqus were used to simulate a low-amplitude wave phenomena in water and solids. The main element shape used in the Acoustic domain is Quad, which uses exclusively quadrilateral elements. Fig. 11 shows an example of a mesh that was used for simulation. To avoid mesh problems with connecting partitions, a Quad-dominated element shape is utilized that also allowed triangles in the transition regions.

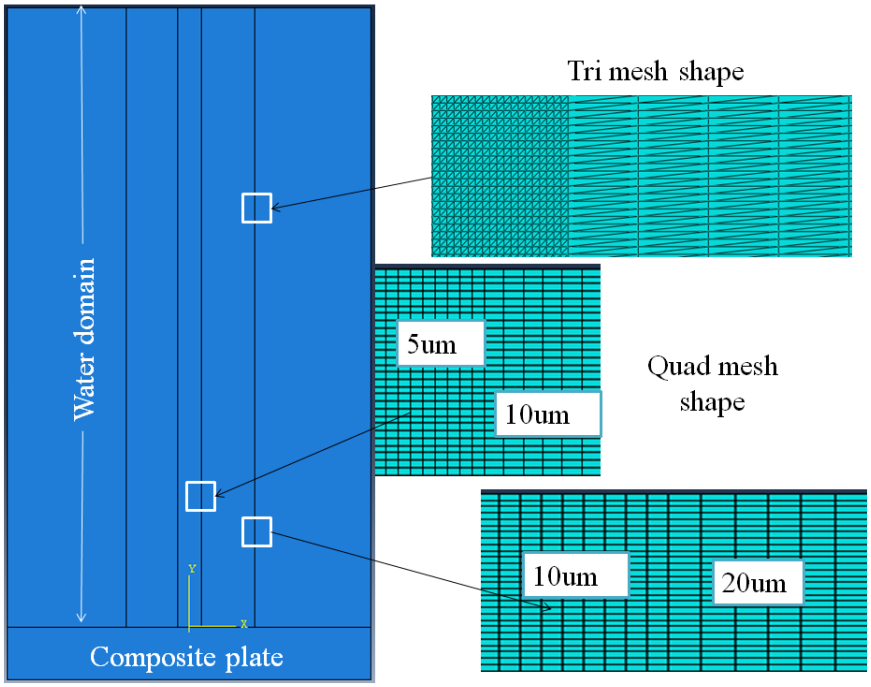

Figure 11. Simulation domain assembly and mesh elelements used for simulation.

6 Finite Element Simulation Results

All of the finite element (FE) simulations are solved in two domains: liquid and solid (solid phantom). Having established the water domain (32mm wide and 50.8mm high) and the composite domain (32mm x 4.47mm), three different cases are simulated. These cases include generation of pressure waves by one probe element and four probe elements. The four probe element generation in turn is simulated for unfocused and focused acoustic beams. The experimental data consisted of three frequencies: 1.0 MHz, 2.25 MHz and 5.0 MHz.

1.0MHz could not resolve desired details due to the relatively large wavelength. The 5.0 MHz signal is able to detect millimeter scale flaws since the propagation into the thin material is adequate. This report will be focused on the case with the

5 MHz (Fig. 8) interrogation pulse. This is because it gives the best results for the fault detection and implies a more challenging case from the simulation point of view.

The first plot (Fig. 12) shows snapshots of the pulse propagation from one element probe at three different times, which hits the composite media and reflects back (displacement in the plate is not presented on the plots). This happens after 35μs as seen on the left plot. The wave is mostly cylindrical except for the lateral edges where the wave practically vanishes due to nonreflecting boundary conditions. Nevertheless, you can still see that the edge reflection effects occur because the edge elements act as point sources generating reflecting waves. The reflected expanding waves are not considered here because they appear as noise when read from the probe element. These reflections can be safely ignored because they vanish for a large simulation domain. For a smaller domain, with 1cm or 2cm width, the amplitude of these reflected waves is larger.

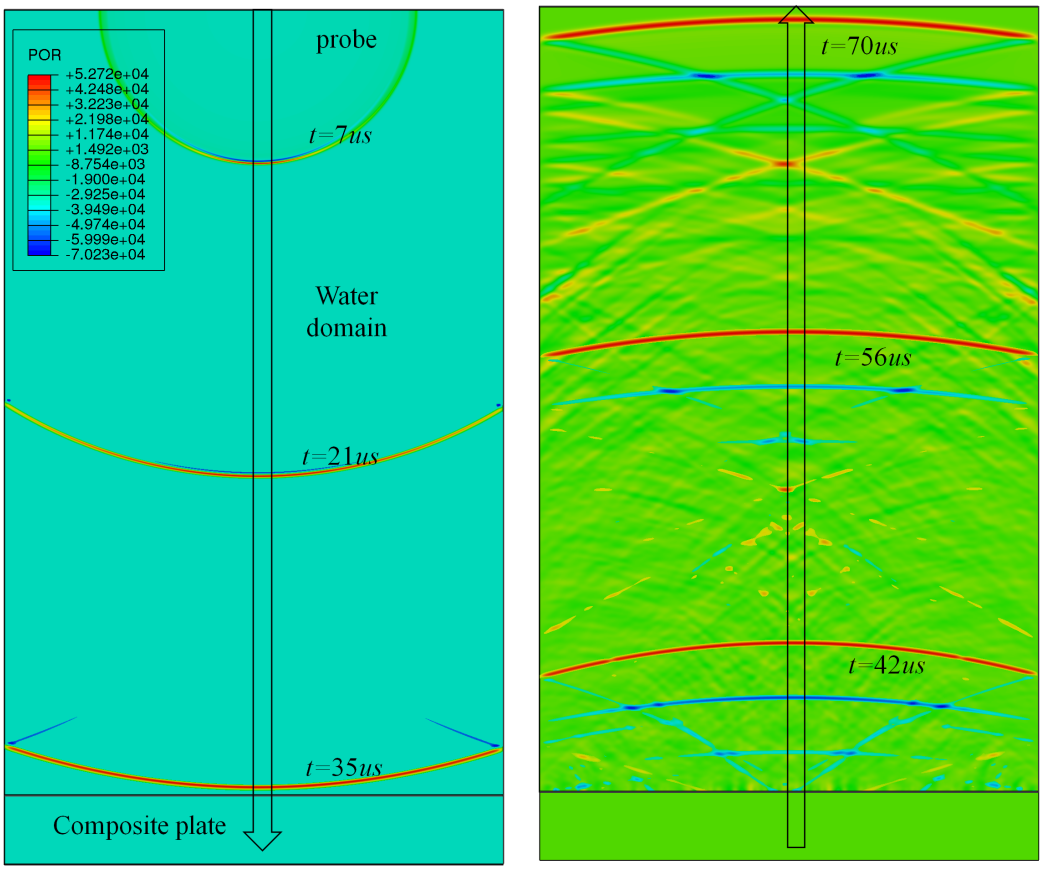

Figure 12. Time snapshots of the water pressure simulation results. The image on the left shows the pulse propagating from the top probe to the composite panel. The image on the right shows the pulse propagating back after the reflections from the panel edges (top and bottom). The arrows show the path that ultrasonic pulse traverses in the FE simulation. Solid phantom is used for simulation.

The snapshot in the middle (Fig. 12) shows the pressure pulses at three different times, as well at the time of the pulse traveling back. At 70μs, the pressure pulse is about to hit the top edge of the water domain. The third snapshot shows the pressure pulse distribution after it reflects from the top edge of the panel. The right hand side plot shows the signal structure in the water domain after recording information on the probe element. In successive plots, snapshots show that the pressure distribution contains all the information of the fault. Integration of the probe signal gives the A-scan signal which can be compared with experiment.

The first row of the plot Fig. 13 shows snapshots of the pulse propagation from the one element probe, at three different times, the wave hits the composite back wall and reflects back. The fourth and fifth snapshots show the pressure pulse (stress) distribution after the reflection inside the composite phantom. The sixth snapshot at $t = 78\mu$s shows a part of the pulse reflecting off the top edge of the water domain. In this case the plate is pristine without any fault (the head is red and the back of the signal is blue with some small amplitude signal mainly due to lateral reflection). The train of signals make a path to the top of water domain where the probe element is located, and then reflects back to the bottom. The second set of plots show snapshots of the wave in the composite phantom. After htting the plate, the signal passes to the free bottom of the plate and then reflects back (time is indicated on the plots). The last plot (top right corner) is the wave distribution after the signal gets reflected from the top of the domain.

The time-domain FE simulation (A scan) shown here, and in other locations of this report, is obtained by averaging the pressure wave over the probe element length. For the 4x4 probe element generation, the central path of the water domain was meshed with 5μm resolution.

The pressure wave distribution for this simulation is presented in Fig. 14. Figures 12 and 14 show the generation of the pressure pulse by 4 simultaneous probe elements. This represents a similar pressure wave distribution with greater amplitude. The spatial structure of the reflection from the top edge is about the same.

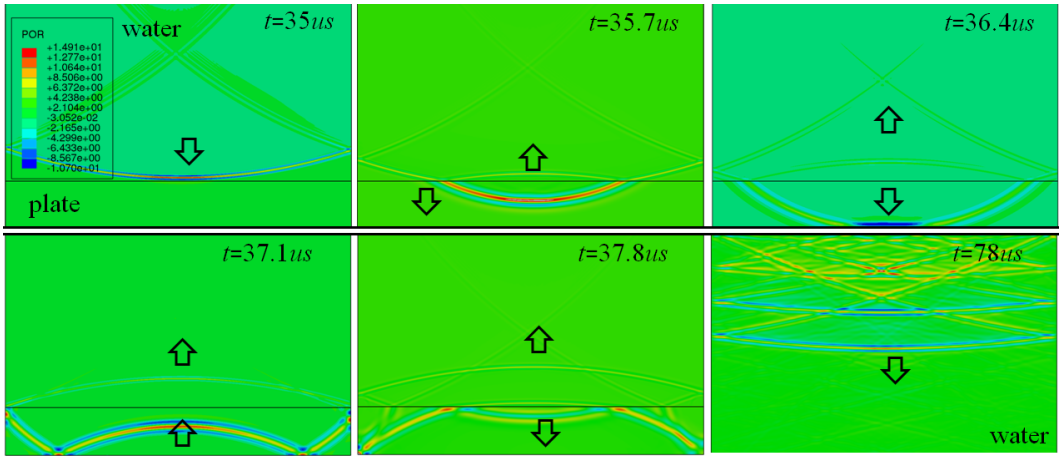

Figure 13. Snapshots of the water pressure simulation results for the acoustic phantom medium. The images on the first row show the pulse propagating from one probe element to the backside of the panel, and the second row shows the image of the pulse propagating back to the top of the water domain. Arrows show the path of how the ultrasonic pulse traverses in the FE simulation.

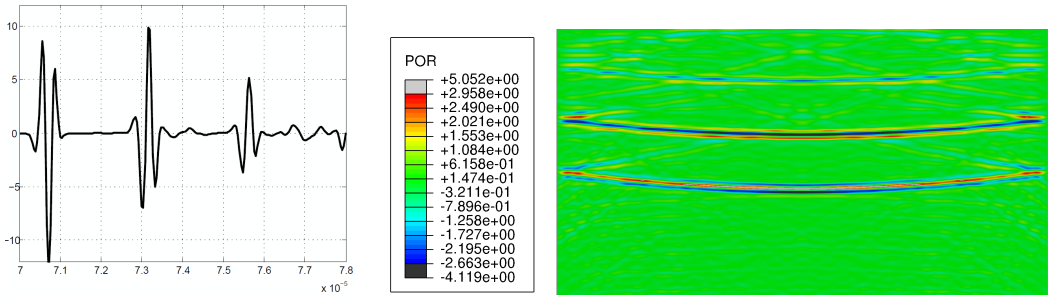

(a) (b)

Figure 14. (a) A-scan signal on the probe simulated for composite plate without delamination (b) snapshot of the pressure wave distribution in the water domain for time t=78μs.

The signal (8) is used for simulation which best reflects the experimental data. The one peak signal simulation results are presented in Fig 15. Using finer mesh size it is possible to obtain a very clean reflection which explains the wave propagation physics. The signal reflects from the bottom of the plate, changes its phase, and between these two signals no oscillations can be seen in the computer simulation. The oscillation after the time of flight are caused by side reflection, as seen from the pressure distribution plot.

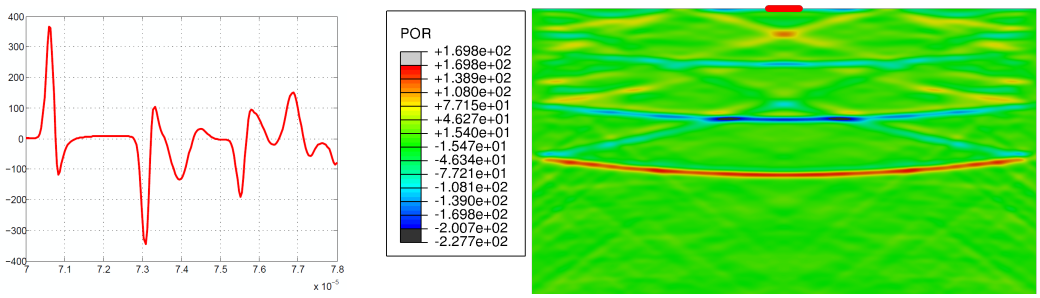

(a) (b)

Figure 15. (a) Ultrasonic pulse at the prob for the plate with a delamiation in the middle. (b) A strong reflection from the dalamination creates a fault signature which is reproduced by FE simulation.

Curved panel simulations are presented in figure 16. For much of the analysis conducted here, the elements within and the ultrasonic probe head itself were small enough compared to the radius of curvature of the composite panel beneath the head to allow for planar simulations. For completeness, the curved geometry was also simulated. As an example FE simulation results are presented for 6 cm radius. Since the saddle panel has more complicated geometry than a planar panel, several simulations were performed with convex and concave shapes of the composite panel. It is easy to see that the simulations do not have much difference from the flat panel. The curvature changes the resulting pulse echo amplitude but it doesn't change the structure of the pressure wave with wavelength λ of about 0.3mm. The first snapshot of Fig. 16 is taken at t = 35μs, showing the pressure pulse that passed the water domain. The signal is sufficiently clean. The second snapshot shows the pressure pulse as it reflects and gets transmitted inside the panel. The third snapshot is at the time t=70μs when the pressure pulse is about to hit the top edge, and the last one on the right shows the pressure wave distribution after reflecting from the top.

The average over the probe length pressure signal (A scan) is showed in the insert of the plot. Since minimum curvature radius is about 5in the inserts for pressure wave distribution show probe signal for such curvature radius compared with the flat panel (blue dashed line) Fig. 16, 17.

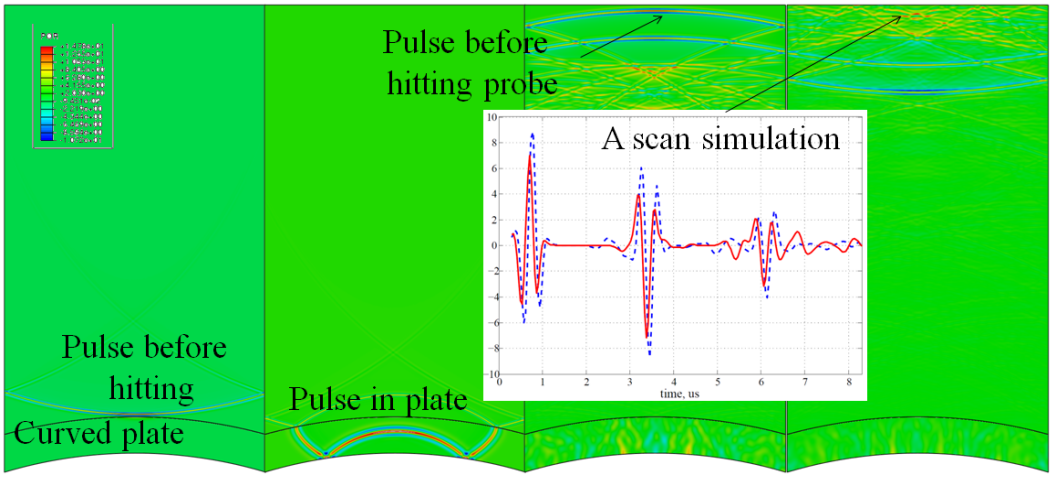

Figure 16. Typical pressure wave propagation in water domain and curved composite panel (convex surface on the water domain side, curvature panel radius 6 cm). The insert shows the amplitude of the pressure wave on the element probe for 5 in curvature radius .

From the FE simulation of the convex and concave panels presented in Fig. 16 and 17, it is easy to see that the amplitude of the pressure wave signal is greater for the concave surface than for the convex one 16.

More importantly, curved panels such as the saddle part considered here (Fig. 1) show the same simulation features as a flat one. This situation changes, however, when the radius of curvature becomes significantly less than the distance to the UT probe. However, this case is not considered here.

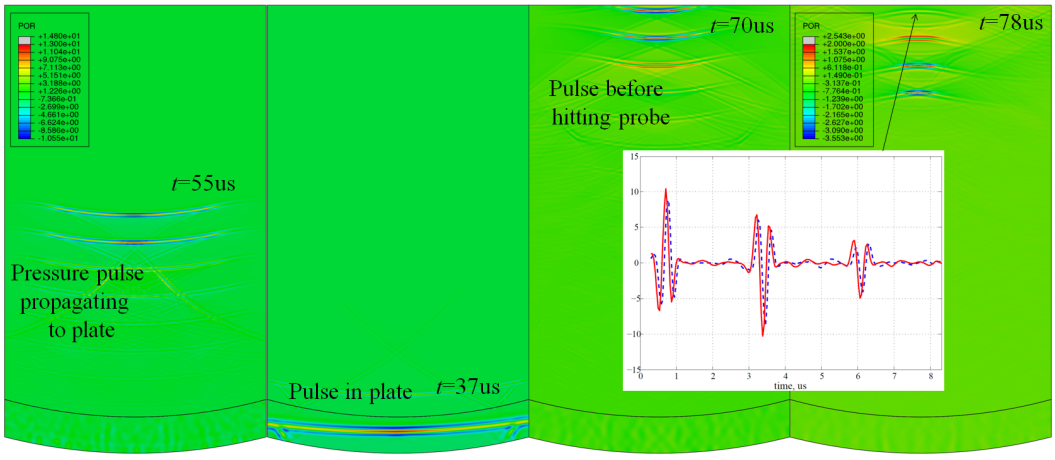

Figure 17. Pressure water propagation in water domain and curved composite panel (concave surface). The insert shows the amplitude of the pressure wave on the element probe.

Rough surface modeling.Pressure wave scattering typically changes with suface roughness. The composite plate surfaces might be rough for IML and OML

tooling. Thus, it is important to understand how the main simulation results will change when taking into account a rough surface. To represent roughness the bond surface of the water domain and the composite one are meshed with a much coarser mesh than the mesh size of the main simulated domains (18). The solid and the water domains are partitioned by introducing a small layer from both sides and a coarse mesh for the connecting layers. In this case, the mesh plays the role of a local inhomogeneity changing the surface scattering mechanism of the pressure waves. As a result, this may change the inspections results. Focused research is required to determine the effect of scattering due to composite surface roughness. For our study, the amount of roughness encountered on the saddle part is not considered typical and therefore did not warrant extensive study.

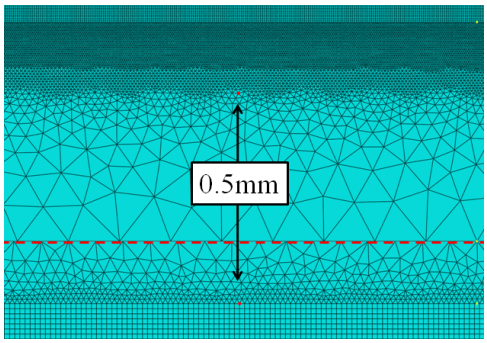

Figure 18. Mesh approach to model roughness at the interface boundary between composite and water (red dashed line).

The FE simulation results for the time-domain pressure wave are shown in Fig. 19. The pressure plot is compared with one obtained for the smooth surface with the same simulation parameters. Despite the probe signal being integrated over the probe element surface, there are more oscillations between the echoes of the reflected signal (from the top and the bottom of the plate).

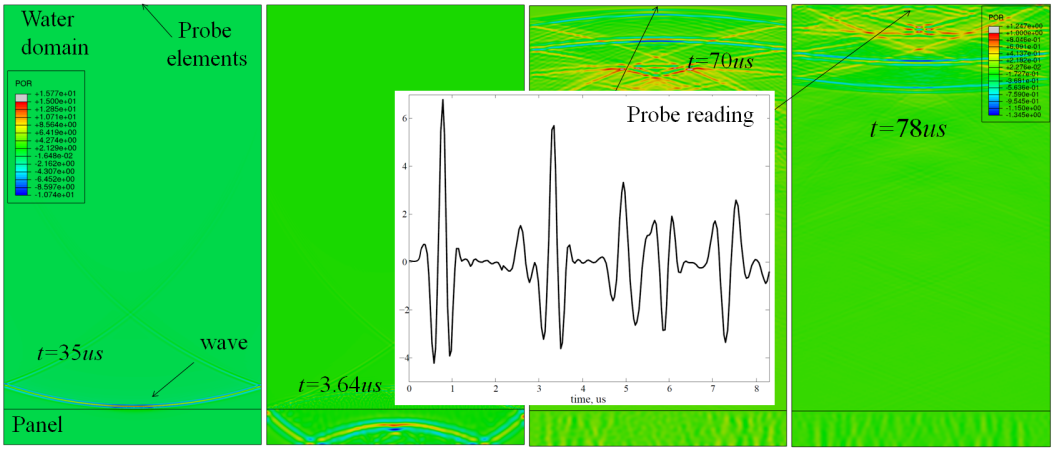

Figure 19. Pressure water propagation in water domain and curved composite panel (concave surface). The insert shows the amplitude of the pressure wave at the probe.

The simulation results of the rough surface (18) when compared to smooth surface results in Figures 14, 16, 17 has greater scattering that contains high frequency oscillations presented in the time-domain insert in Fig. 19.

7 Simulation of Faults

Fault detection. One goal of ultrasonic interrogation is to determine the location, shape and size of possible faults. The transducer excitation pulse interrogates the system and the output of the system response is the shape of the echoes read by the probe elements. The main system parameter is the time-of-flight and the amplitude of the back-scattered signal. In addition to the backscattered signal considered above, there is an inhomogeneity or discontinuity causing a reflected signal. With any local layered material changes, local discontinuity results in the generation of additional reflected signals. In an experiment, the location and size of the flaw can be evaluated with an A-scan signal. This method is most sensitive to the delamination detection since the impedance difference between solid and air is very significant. Moreover, in layered composite materials, laminate delaminations are the major faults. The natural question comes up as to what size delamination reflects the incident energy of the pulse. Since delamination of interest are on the order of microns, they are typically larger than the wavelength of the interrogation signal. This problem is discussed in [6]. In this approach the amplitude motion in the composite is determined by the relation:

$$\xi = p/(Z\omega)$$

where p is the sound pressure, $\omega = 2\pi f$ is the angular frequency, ξ is the particle displacement and c is the velocity of the sound in the medium. With the intensity of the sound:

$$J = \frac{p^2}{2Z} = \frac{Z\omega^2\xi^2}{2Z}$$

Giving

$$\xi/\lambda = \sqrt{J/(2\pi^2\rho c^3)}.$$

Substituting known parameters for a 5MHz signal, the ratio ξ/λ becomes 1e-6, which means that any delamination can be considered as a surface with air and free boundary.

We will primarily consider delamination discontinuities where the two close sides of a crack are not connected. The fault is located at the center of the plate, and it will be interrogated by a UT pressure wave that strikes the plate in the perpendicular direction. Then the fault is moved from the center of the composite to the surface of each external boundary of the plate in order to understand how the shallow delamination can be revealed.

Plots 20 compare the simulation of a single element pressure wave generation in a pristine plate with one that has a fault located at the top. These snapshots are different. The plot shows that a 3mm long fault near the top boundary of the plate changes the pressure distribution substantially. The pressure wave reflection from the top of the plate is about the same, although the echo signals are completely different.

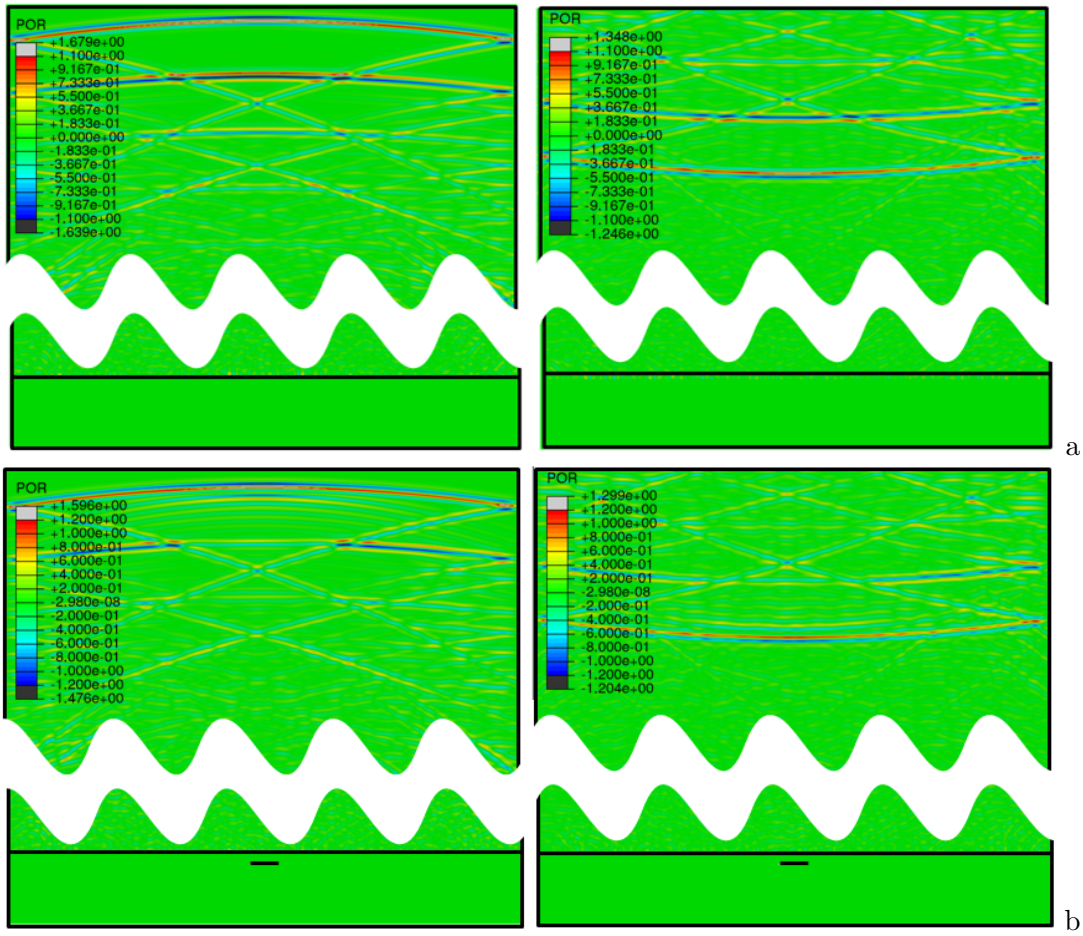

Figure 20. Snapshots of a pressure pulse reflecting from the top surface without fault (a) and with a fault close to the surface (b). The pulse wave was generated and received from a single element probe.

The magnified view of the simulated UT pulse propagation and scattering for a fault positioned deeper in the composite material is presented in Fig. 21,22,23. The left hand side snapshots display the acoustic pressure, and the insert magnifies the pressure distribution at the specific time displayed on the plot. The first magnified view of the simulated UT pulse is presented in Fig. 21. It shows that the pulse is about to impinge the plate and does not reflect any fault features at all. Fig. 22 shows the pressure pulse before impinging the top and how it is different from the pristine pressure plot case. In Fig. 23 the pulse is reflected back and is not very distinguishable from the homogeneous plate signal because the fault is too shallow and it is located on the back side of the panel.

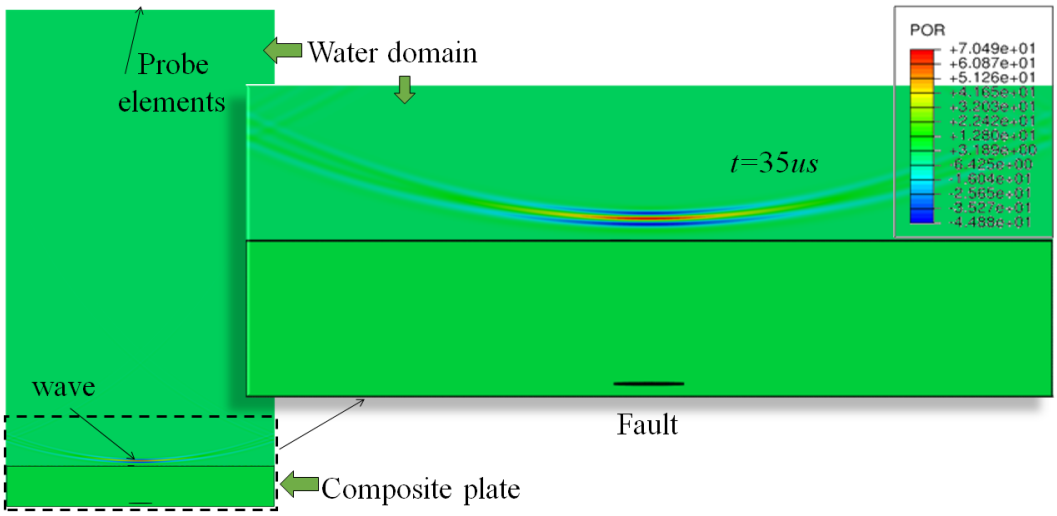

Figure 21. FE simulation of the pressure pulse propagation in water domain at t=35μs. The insert shows the details of the pressure wave.

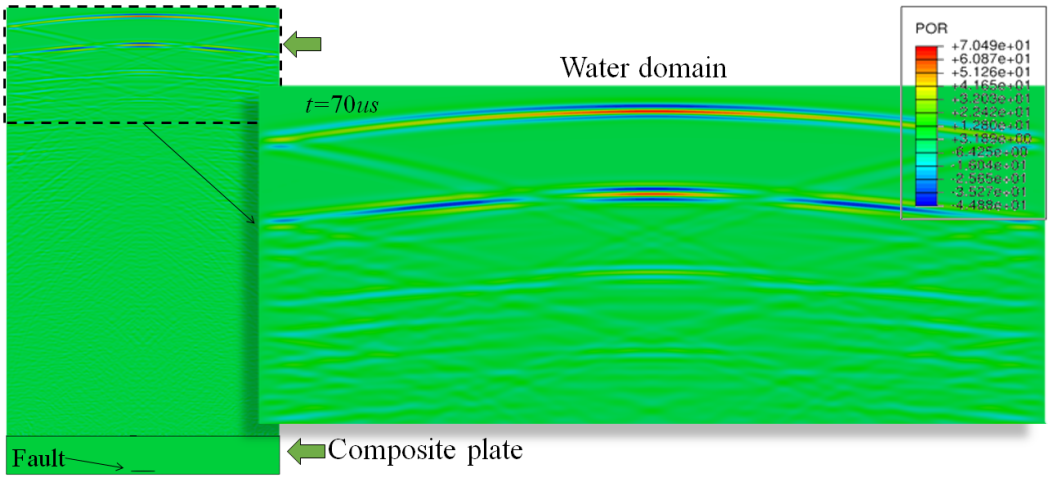

Figure 22. FE simulation of the pressure pulse propagation in water domain at t=70μs. The insert shows the details of the pressure wave.

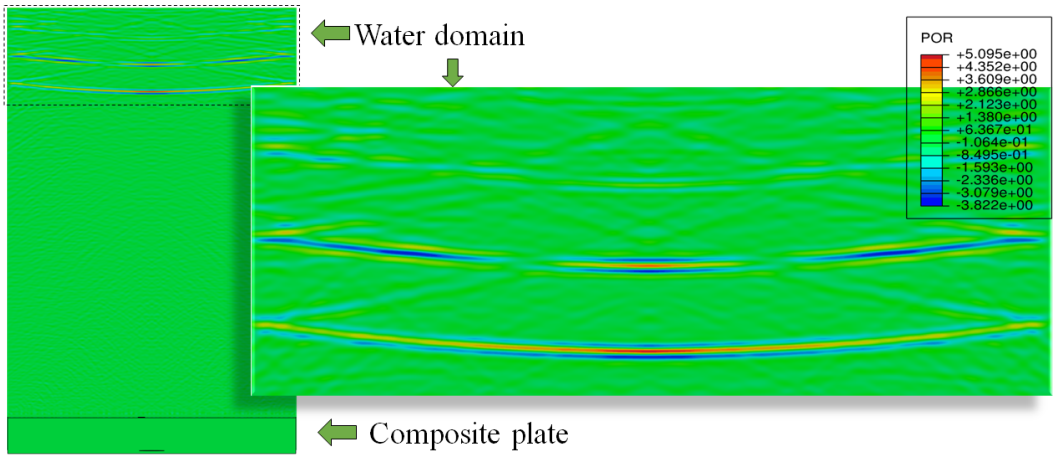

Figure 23. FE simulation of the pressure pulse propagation in water domain at t=78μs. The insert shows the details of the pressure wave.

The results of the FE simulations for the delamination at the top of the plate are presented in Fig. 24.

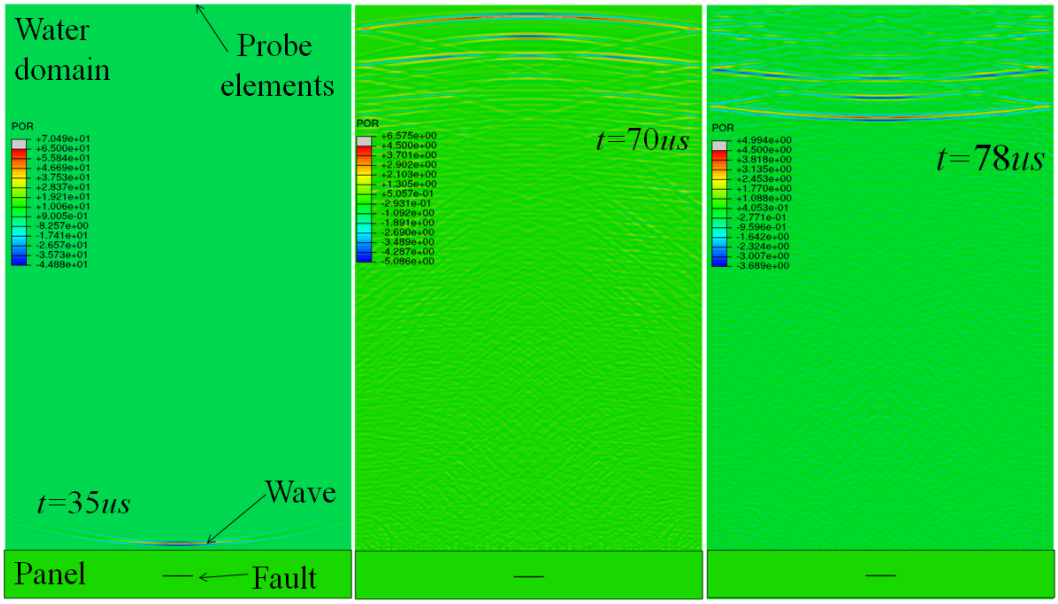

Figure 24. FE simulation of the pressure pulse propagation in water domain with the fault on the top of composite plate.

The reflecting pressure feature is understood by the A-scan plot presented in Fig. 25. The snapshot next to the time-domain plot explains the pressure distribution after reflection. The simulation is performed for 4x4 probe elements. The multiple paths of the reflections from the bottom edge and the delamination presented in the figure strongly correlate to the fault location and the back side of the panel.

The time of flight characterized by rising peaks reflects the fault signature, and strongly depends on the depth of the delamination. Note that there is noise in the signal and pressure wave distributions from the lateral reflections. The Figure 25 shows the UT propagation in the water-composite domains with a delamination in the middle of the plate. The depth of the delamination is about 40% from the top surface of the plate. As can be seen from this plot, the generated A-scan picks up the pulse reflected from the delamination. Also as the time goes on, the pulse propagates further along the thickness until it is reflected from the back side. Then the secondary reflection can be seen from the delamination, etc.

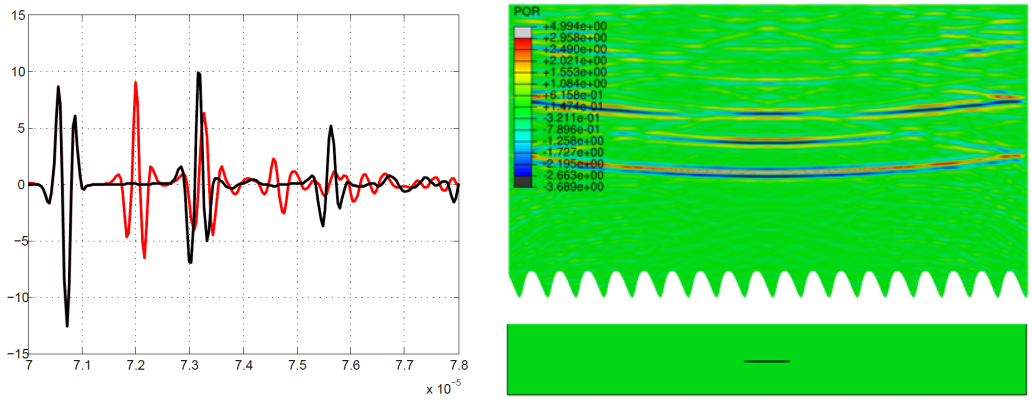

(a) (b)

Figure 25. (a) Time-domain signal recorded at the probe for delamination in the middle of the plate – (b) and Corresponding pressure wave distribution in the simulation domain (actual fault location is displayed below the pressure distribution).

Figure 26 shows a fault created where by one ply (3mm length, thickness 0.15mm) at the center of the plate is substituted with matrix epoxy. The amplitude of this signature is smaller than from the delamination. This can be seen as well in a contour pressure distribution obtained from the FE simulation plot on the right. The matrix fault signal feature is barely visible on the plot.

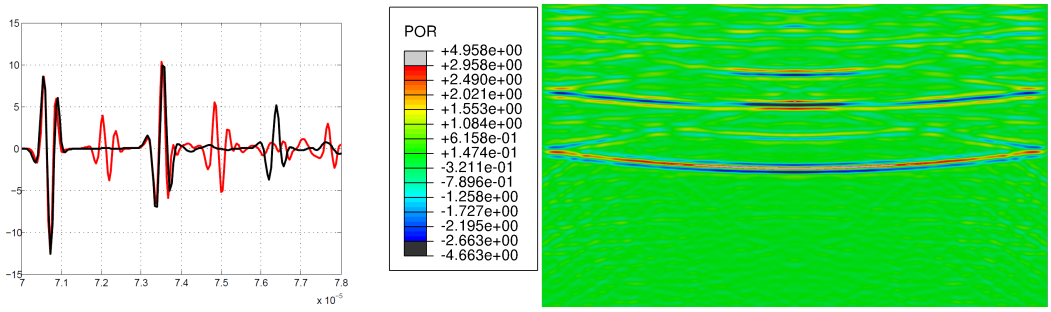

(a) (b)

Figure 26. A-scan signal simulated for the composite plate with a fault of one ply replaced by epoxy matrix 3mm wide.

The influence of the delamination depth on the time-domain signal is obtained. Several different crack depth locations are presented in Figure . The delamination in the area near the middle of the plate has a good fault signature since pulsed echo signals from the fault and back side of the plate are separated in time.

Simulations were used to evaluate the hypothetical fault signal and pressure wave distribution in the water domain for different locations of the fault. The simulation of wave propagation in a solid system with a small fault is carried out by the same approach. The finite element method simulation of these cases is presented in Fig. 8. An additional peak associated with the delamination position is shown in A-scan plot, as well as in the pressure distribution in the water domain. For a shallow fault in the vicinity of the boundary the peak of the reflection moves to the corresponding boundary.

For the second simulation sample, the delamination is located close to the back side of the plate as shown in Fig. 27, 28. The size of the delamination is about 2mm. Figure 27 shows that the first echo is the reflection from the top edge rather than from the delamination, and the last echo is the back-edge reflection. Since the delamination is too close to the bottom surface (shallow delamination 10% in depth from the bottom) more sophisticated signal processing is required to discern the fault close to the plate surface.

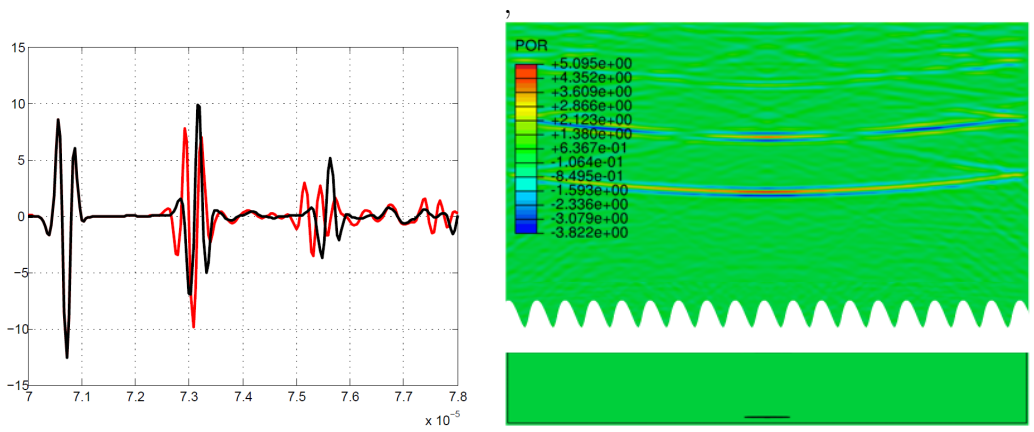

(a) (b)

Figure 27. (a) The time-domain results obtained from the probe element, (b) contour plot of the pressure waves on the top of water domain.

The time-domain plots obtained from FE simulations for the delamination close to the top of the surface are presented in Fig. 28.

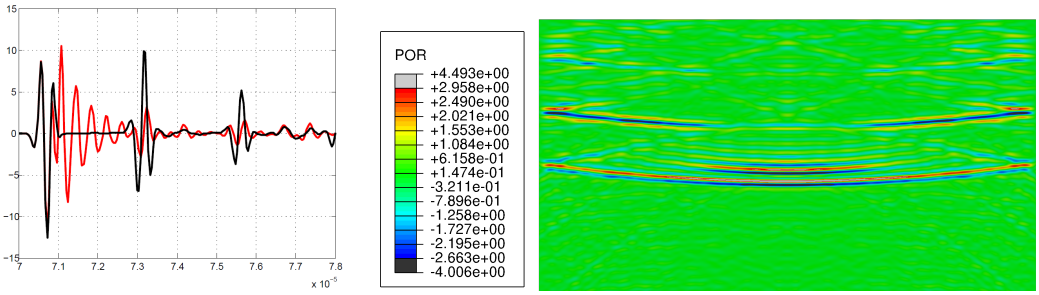

(a) (b)

Figure 28. (a) A-scan signal on the probe simulated for composite plate with delamination located 0.15% under the surface, (b)snapshot of the pressure wave distribution in the water domain for t=78μs.

All of these signals are different from the signal of the virgin plate. However, from the detectability point of view, it is not always possible to discern these features. For example, the bottom delamination, which is located ten percent from the bottom of the plate, is not easily discernble in the experiment. Analyzing the reflection signal from the viewpoint of experimental detectability, this depth should be at least 0.15% for the thin composite panel (5mm and frequency 5MHz).

Delamination size variation

The pressure wave obtained by the focused array is practically the same as the one generated by the 4 element array generating a planar pulse via simultaneous firing. Figure 20 shows similar results for the bottom fault location. The whole

domain is on the left, and the magnified domain plot is in the insert. The distribution of the pressure wave in the water domain before striking the plate is the same (left plot). After reflecting back, the signals are different on the probe elements depending upon the fault location Fig. 29

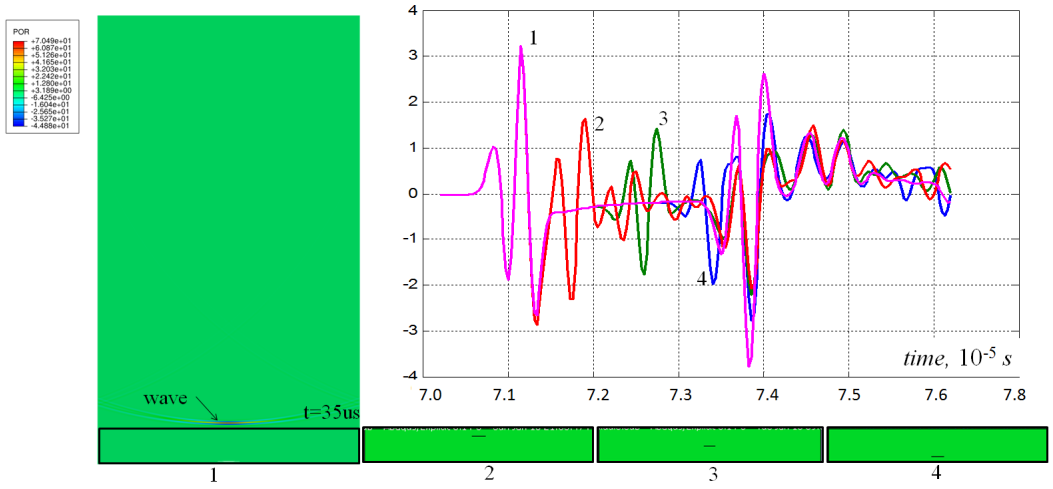

Figure 29. The simulation domain for different fault locations in the plate (plate is shown on the bottom and numbered from 1 to 4). Time-domain plots averaged over 4 probe elements are presented on the same plot.

The dependence of the pressure reflection signature on the delamination size can be determined from the plots 25 for 2.7mm delamination size located 2mm from the bottom, and from the next simulation in Fig. 30 for an 800μm length fault. The 800μm fault demonstrates that it is possible to determine such a fault size using a 5MHz signal. The length of 800μm is comparable with the wavelength of a 5 MHz signal which is 0.6mm. With more sophisticated signal processing it should be possible to detect even smaller defects.

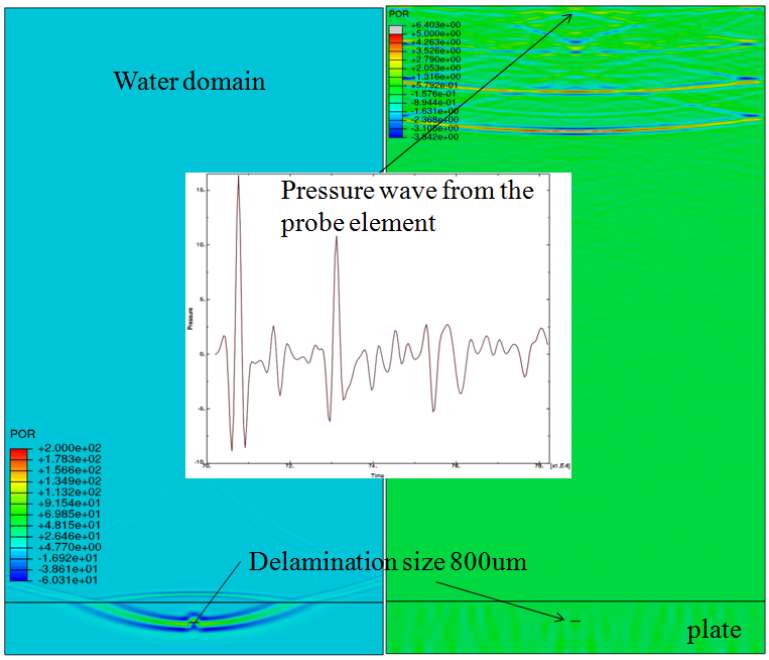

Figure 30. The simulation of the pressure reflection for an 800μm fault length, the insert shows the corresponding A-scan.

As previously discussed, the amplitudes of the transmitted and reflected waves can be determined from the impedance relation ($Z = \rho c$). Following the physics-based analysis for a 1D plane wave consideration (Section 3), the reflection from the delamination is the same as the reflection from the backside wall considering that this local wall is closer (the place where the delamination is localized) to the top surface.

In our 2D or 3D simulation the delamination size is equal to or greater than the wavelength. In this case, part of the energy is reflected from the delamination while another part is reflected from the backside. Depending upon the size of delamination, different signatures can be observed from the delamination. By FE simulation, the probability of flaw detection can be quantified with decreasing flaw size. The characteristic results of detectability of delaminations are presented in Fig. 31, 32.

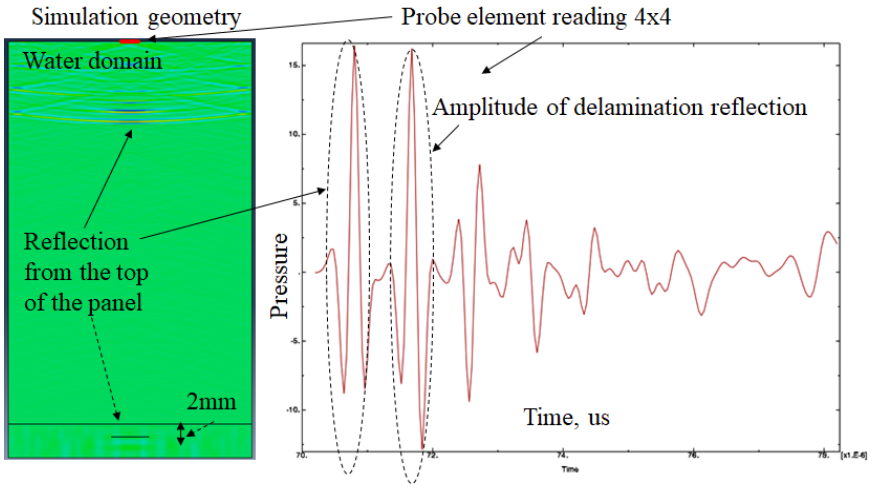

Figure 31. A typical A-scan signal with a reflection from the delamination used for plotting Figure 32.

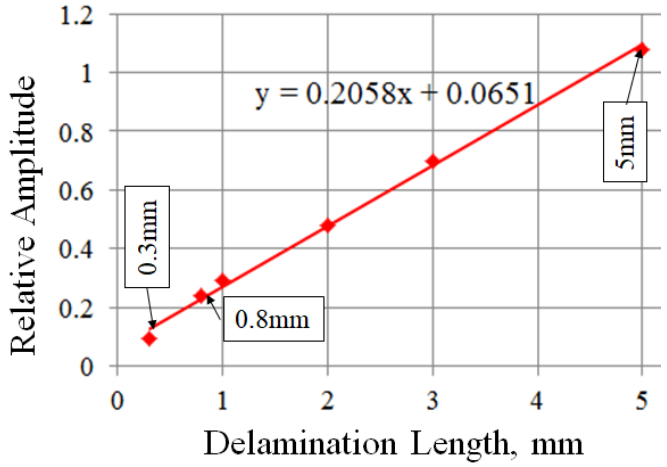

Figure 32. Relative reflection amplitude versus delamination length. The relative amplitude is the peak-to-peak amplitude of the wave reflected from the delamination divided by the peak-to-peak amplitude of the wave reflected from the top surface. The fault was located in the middle of the panel.

The results show that a delamination flaw located in the middle of the plate can be detected down to a size of about 300μm. Formally, a minimum detectable defect size has not been identified because it depends on the signal to noise ratio of the measurement instrumentation. At the same time, the trend-line in the delamination size plot makes it possible to find a ratio of the delamination backscattered signal to the surface reflected signal for any possible delamination size (Fig. 32). On the figure, the relative amplitude of the fault detection can be seen, which is determined as a ratio of peak-to-peak amplitude of the delamination signal to peak-to-peak

amplitude of the top surface reflection. The trend-line shows the approximate value of the relative amplitude at the give delamination size. The curve starts from the 300μm delamination size up to a 5mm.

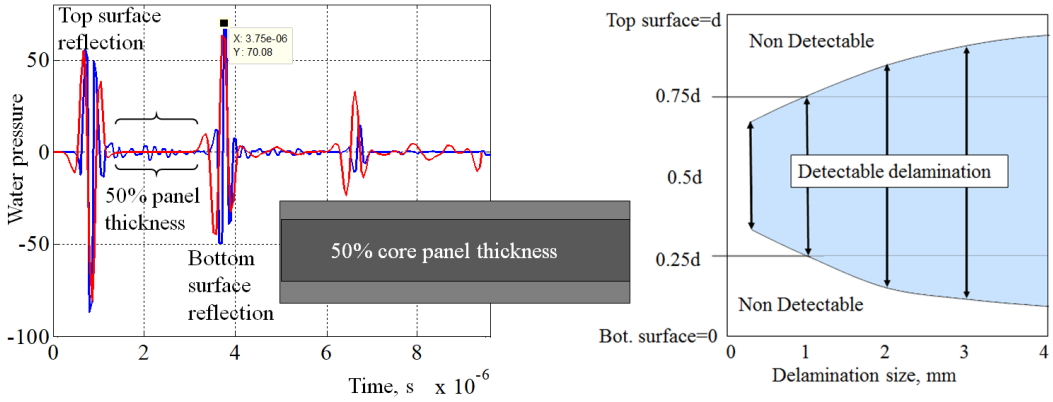

Figure 33. Qualitative analysis of the fault detectibility obtained as a result of simulation.

The typical interrogation pulse length in our simulated A-scan plots is about 8μs. This was a bit larger than the pulse length in real experiments. This is due to the mesh size limitation which in our case was about 5μm. In this case, the dispersion property causes the simulated signal propagation to become a bit wider than the experimental one. The time of flight between the top surface and backwall scattering is about 30μs (Fig. 33). As a result, the temporal scale separation is about a factor of 4. This means in general, signals from a delamination located in the middle part of the panel, at 50% of the thickness depth and 25% from the walls, will be not masked or disrupted by the wall reflections. As a result, the fault can be discerned if the delamination is closer to the middle of the thickness. The signal from this delamination will be between the two first peaks separated by wall reflections (Fig. 33, left). As the depth of the delamination increases from the surface, a more pronounced delamination signal is obtained. If the delamination is located in the shallow region from the boundary, the signal starts to interfere with the boundary reflection and the probability of discerning this fault decreases. FE simulation shows that fault detection of the delamination at 5MHz even when the fault is near the surface, can be detected even at 10-15% depth from the surface. Detectability depends upon the fault size as well. A view of the delamination detectability is presented in Fig. 29, 33. A tradeoff for fault detection is that the larger the delamination, the more pronounced is the delamination signature. The smaller the size of the delamination is then the closer it needs to be to the middle of the panel thickness for detectability. Moreover, the delamination located near the top surface is easier to identify than the one located at the same distance on the bottom surface. This indicates that imaging should be done on both sides of a panel if it is desired to detect near surface faults.

8 Experimental Verification of the Fault Detection

The simulation results can be fitted to show that the simulation approach is self-consistent with the results of UT scans. Taking several paths (with the y value certain), it is possible to reproduce the A-scan plots and explore how they can be fitted by amplitude plots on the element probe.

The delamination depth through simulation with a hypothetical fault is considered. The effect of varying delamination depth is shown in Figures 34,35,36. The simulation shows a pronounced reflection in all simulations despite the fact that the size of the fault was about 3mm or less. This is because the stress (pressure) waves fully reflect from the delamination due to the high impedance difference between air in the delamination and the composite. At the same time the impedance ratio between the carbon and the epoxy matrix is much smaller. As a result, the reflection from a matrix inclusion isn't so pronounced.

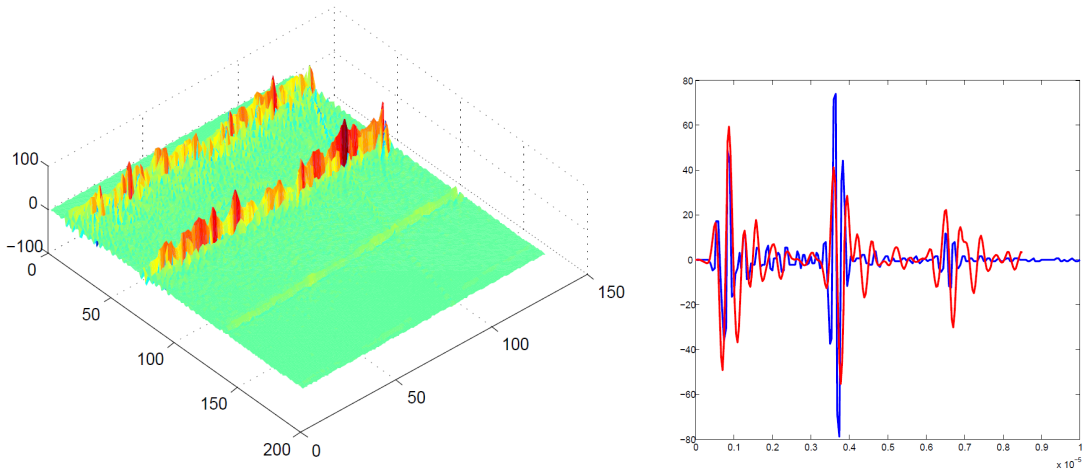

(a) (b)

Figure 34. (a) Experimental B-scan of the saddle plate showing strong reflection from the edge of the late. Experimental results for different fault locations, (b) comparison experimental (blue curve y=111) with FE simulation results (red curve) - b).

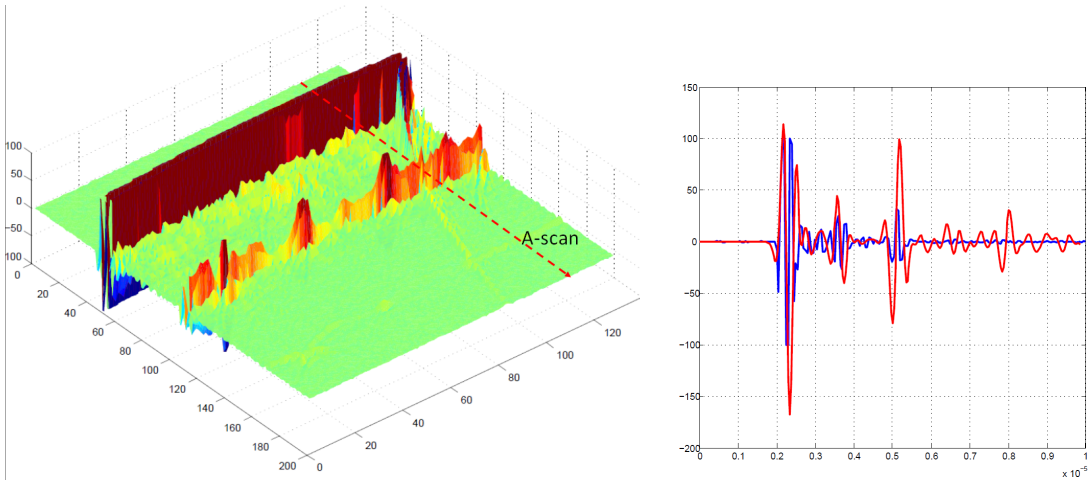

(a) (b)

Figure 35. (a) Experimental results for different locations, (b) comparison of experimental (blue curve y=97) with FE simulation results (red curve).

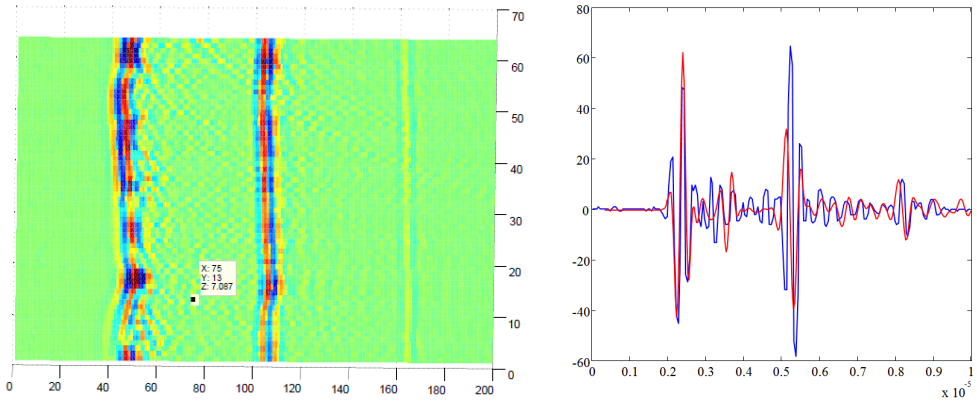

(a) (b)

Figure 36. (a) Experimental results for different locations, (b) comparison experimental (blue curve taken for y=13) with FE simulation results (red curve).

Finally, the FE simulations and the comparisons with experimental data show successful modeling of the UT scan features. The numerical results show that the approach is feasible and effective for experimental data interpretation.

9 Conclusions

An Abaqus finite element model is developed for simulation of ultrasonic interrogation of a composite material in a water domain. The proposed model is based on realistic geometry of the experimental setup including the ultrasonic probe elements which were used in the experiment. Despite the fact that the high frequency probe interrogation requires sufficiently high mesh resolution, the task was successfully accomplished by simplifying the simulation approach using physics-based analysis. As a result, the simulated ultrasonic signals of the A-scan show good agreement to the experimental signal.

Computational simplifications included simulating in 2D instead of 3D, and introducing a phantom medium for the composite plate. The characteristic feature of the phantom medium is that it represents the acoustic properties of the composites required for accurate comparison with experiment. Many computational tests were realized to reproduce the experimental results. The present approach has demonstrated that it can be used for calculating A-scan signals from ultrasonic testing.

It was shown that Abaqus finite element models produce accurate results for a water domain with a solid composite system. Experimental and numerical results agree well. FE simulation is a convenient tool for designing and assessing inspection technique features. A localized fault in any location may be studied to predict the signature of reflections.

The numerical simulation is successfully compared with experimental data containing faults. The developed model can be extended to incorporate additional complexity such as different liquid couplants, temperatures, surface roughness and part geometries.

There are two main outcomes from this study. The first is the detectability with respect to depth of delamination. If a delamination fault is too close to the front surface or the back surface (e.g. within 15% of total thickness), then the signal will be confused with front and back side reflections. This may in part be mitigated by interrogating both sides of the panel. Secondly, if the fault is too small with respect to the interrogation wavelength, the fault reflection signature will most likely be lost. For this composite material with 5MHz interrogation frequency, faults less than approximately 1mm may be difficult to detect without further development of appropriate inverse models.

10 Acknowledgments

Stefan Schuet is to be sincerely thanked for providing many helpful comments.

References

1. Olympus User Manual Focus PX Phased Array and Conventional Ultrasonic Data Acquisition Instrument , DMTA-20090-01EN, Rev. D, October, 2017, Olympus Scientific Solutions, Waltham, MA.

2. Lester W. Schmerr, Jr. Fundamentals of Ultrasonic Nondestructive Evaluation A Modeling Approach. Second Edition. Springer International Publishing Switzerland 2016.

3. Pietro Burrascano, Sergio Callegari, Augusto Montisci, Marco Ricci, Mario Versaci. Ultrasonic Nondestructive Evaluation Systems. Industrial Application Issues. Springer International Publishing Switzerland 2015.

4. J. David N. Cheeke. Fundamentals and Applications of Ultrasonic. CRC Press LLC. 2002.

5. Subhendu K. Datta, Arvind H. Shah Elastic Waves in Composite Media and Structures With Applications to Ultrasonic Nondestructive Evaluation. 2009 by Taylor and Francis Group, LLC

6. J. Krautkramer and H. Krautkramer, Ultrasonic Testing of Materials, Springer-Verlag, 1990.

7. Abaqus user manual. http://130.149.89.49:2080/v6.7/books/usb/default.htm?startat=pt05ch17s01.html

Appendix A

Parameters

Table A1. Material play parameters of IM7/8552

Material parameters of IM7/8552	**Symbol**	**Value**
Density, kg/m^3	ρ	1570
Young modulus, GPa	$E_1,\ E_2,\ E_3$	170.00, 9.80, 9.08
Poisson's ratio	$\nu_1,\ \nu_2,\ \nu_3$	0.32, 0.32, 0.50

REPORT DOCUMENTATION PAGE

Form Approved
OMB No. 0704–0188

1. REPORT DATE *(DD-MM-YYYY)*	2. REPORT TYPE	3. DATES COVERED *(From - To)*
01-03-2019	Technical Memorandum	

4. TITLE AND SUBTITLE
Computational Non-destructive Evaluation Improving Ultrasonic Interrogation of Complex Geometry Composite Parts

5a. CONTRACT NUMBER

5b. GRANT NUMBER

5c. PROGRAM ELEMENT NUMBER

6. AUTHOR(S)
Vasyl Hafiychuk, Kevin R. Wheeler, Ken Gee

5d. PROJECT NUMBER

5e. TASK NUMBER

5f. WORK UNIT NUMBER

7. PERFORMING ORGANIZATION NAME(S) AND ADDRESS(ES)
NASA Ames Research Center
Moffett Field, California

8. PERFORMING ORGANIZATION REPORT NUMBER
L–

9. SPONSORING/MONITORING AGENCY NAME(S) AND ADDRESS(ES)
National Aeronautics and Space Administration
Washington, DC 20546-0001

10. SPONSOR/MONITOR'S ACRONYM(S)
NASA

11. SPONSOR/MONITOR'S REPORT NUMBER(S)
NASA/TM–2019–220197

12. DISTRIBUTION/AVAILABILITY STATEMENT
Unclassified-Unlimited
Subject Category
Availability: NASA STI Program (757) 864-9658

13. SUPPLEMENTARY NOTES
An electronic version can be found at http://ntrs.nasa.gov.

14. ABSTRACT

Finite element simulation was employed in modeling the ultrasound (UT) pressure pulse propagation through a coupled liquid-composite medium to reproduce experimental data. From the simulation point of view, the proposed approach is challenging when there is a large simulation domain. For example, it is shown that a sub-micron wavelength of an ultrasonic wave requires a mesh size of several microns and this in turn requires significant computational resources, as well as special care in modeling. Some of the simulation results are presented considering that such modeling should reproduce experimental data for a healthy and faulty composite structure with complex geometry. Many possible experimental setups are simulated to demonstrate the non-destructive testing technique. This setup includes the generation of pressure pulse propagating through the tested composite plate and possible scattering by discontinuities (area of different impedance) that may be present in the panel. This scattered pulse together with the baseline pressure pulse generates a signature on the probe element which can be used to locate the position of defects in the structures.

15. SUBJECT TERMS
CFD, grid

16. SECURITY CLASSIFICATION OF:			17. LIMITATION OF ABSTRACT	18. NUMBER OF PAGES	19a. NAME OF RESPONSIBLE PERSON
a. REPORT	b. ABSTRACT	c. THIS PAGE			STI Information Desk (help@sti.nasa.gov)
U	U	U	UU		19b. TELEPHONE NUMBER *(Include area code)* (757) 864-9658